

Graphical Abstract

Robustness of complexity estimation in event-driven signals against accuracy of event detection method

Marco Cafiso, Paolo Paradisi

Highlights

Robustness of complexity estimation in event-driven signals against accuracy of event detection method

Marco Cafiso, Paolo Paradisi

- The estimation of temporal complexity is robust with respect to the presence of false positives in the event detection method.
- A counter-intuitive result is that, in the range of power exponent μ less than 2.5 the accuracy in the evaluation of diffusion scaling H improves as the number of false positives increases.

Robustness of complexity estimation in event-driven signals against accuracy of event detection method

Marco Cafiso^{a,b,*}, Paolo Paradisi^{b,c,*}

^a*Department of Physics 'E. Fermi', University of Pisa, Largo Bruno Pontecorvo
3, Pisa, I-56127, , Italy*

^b*Institute of Information Science and Technologies 'A. Faedo', ISTI-CNR, Via G. Moruzzi
1, Pisa, I-56124, , Italy*

^c*BCAM-Basque Center for Applied Mathematics, Alameda de Mazarredo
14, Bilbao, E-48009, , Basque Country, Spain*

Abstract

Complexity has gained recent attention in machine learning for its ability to extract synthetic information from large datasets. Complex dynamical systems are characterized by temporal complexity associated with intermittent birth-death events of self-organizing behavior. These rapid transition events (RTEs) can be modelled as a stochastic point process on the time axis, with inter-event times (IETs) revealing rich dynamics. In particular, IETs with power-law distribution mark a departure from the Poisson statistics and indicate the presence of nontrivial complexity that is quantified by the power-law exponent μ of the IET distribution. However, detection of RTEs in noisy signals remains a challenge, since false positives can obscure the statistical structure of the underlying process. In this paper, we address the problem of quantifying the effect of the event detection tool on the accuracy of complexity estimation. This is reached through a systematic evaluation of the Event-Driven Diffusion Scaling (EDDiS) algorithm, a tool exploiting event-driven diffusion to estimate temporal

*Corresponding author

Email addresses: marco.cafiso@phd.unipi.it (Marco Cafiso), paolo.paradisi@cnr.it (Paolo Paradisi)

complexity. After introducing the event detection method RTE-Finder (RTEF), we assess the performance of the RTEF-EDDiS pipeline using event-driven synthetic signals. The reliability of the RTEF is found to strongly depend on parameters such as the percentile and the number of false positives can be much higher than the number of genuine complex events. Despite this, we found that the complexity estimation is quite robust with respect to the rate of false positives. For the power-law distributed IETs with $\mu \leq 2.5$, the second moment scaling H appears to even improve as the rate of false positives increases, reaching estimation errors of about 4 – 7%.

Keywords: Temporal complexity, intermittency, diffusion scaling, rapid transition events, power-law, noise in signal processing

PACS: 05.40.–a, 05.40.Fb, 05.45.Tp, 05.65.+b, 05.40.Ca

1. Introduction

The present-day focus on data science is linked, on the one hand, to the great availability of huge datasets and, on the other hand, to the increased computational power that makes it possible to use machine learning methods on these same datasets. In this framework, complexity is living a renewed interest due to the need for extracting synthetic information from the large amount of available data [1, 2].

A complex system consists of many interacting elements, or nodes in a network, with nonlinear, cooperative dynamics that give rise to emergent, self-organized, structures, typically displaying some coherence among different elements and in time [3]. This coherence property can be quantified by proper *complexity* measures, or *metrics* in the information science jargon, computed from data that are obtained by observational probes embedded in the complex system. Complexity measures are often referred to the topological properties of the emerging coherent structures and are investigated in the framework of complex networks [4, 5, 6, 7], with wide and interesting

applications in the field of neuroscience [8, 9, 10, 11, 12, 13, 14, 15, 16]. However, when dealing with time evolving systems, e.g., time-varying networks, each network node is represented by a temporal signal. In this case, the investigation focus is also on the temporal dynamics of the network and, thus, on the temporal evolution of self-organized emerging states [17, 18]. Actually, the cooperative dynamics of a wide set of complex systems trigger the emergence of coherent, or self-organized, structures that are not equilibrium states of the system, but, on the contrary, display peculiar metastability characterized by random lifetimes [19, 20, 21, 22, 23]. The complex metastability of these coherent states is a condition that is referred to as Temporal Complexity (TC) [17, 24, 25, 26] or Intermittency-Driven Complexity (IDC) [18, 27]. In this case, the self-organized structures are not equilibrium states but are characterized by a lifetime after which the instabilities of the nonlinear interactions determine a rapid decay of the self-organized state. After that, the system experiences a transition, typically a fast one, to a new dynamic condition, which may be another self-organized state or a disordered state. The latter case is clearly defined by the absence of well-defined internal coherence, whereas, on the contrary, a self-organized state is represented by a state with high internal coherence, e.g. long memory and/or long-range correlations between nodes. The overall displayed behavior is that of a sequence of intermittent events marking the transition among different dynamical regimes. It is essential to emphasize that transitions between self-organized states or between high and low coherence phases are often so fast as to be reduced to an instant in time. In this framework we can introduce the concept of Rapid Transition Event (RTE), and the temporal sequence of RTEs can be modelled as a stochastic point process in the time axis [28], a concept that was largely exploited in brain studies [19, 20, 29, 30, 31, 32]. A point process is mathematically represented as a set of strictly increasing time instants $\{t_n; n \in \mathcal{N}\}$, being \mathbf{N} the set of

integer numbers $n \geq 0$. The most important features of the intermittent birth-death process of self-organizing behavior are then the Probability Density Function (PDF) $\psi(\tau)$ computed from the sequence of Inter-Event Times (IETs) $\tau_n = t_n - t_{n-1}, n \geq 1$, and the statistical dependence among RTEs and, consequently, among IETs. The *renewal* condition, which is defined by the mutual independence of IETs in the point process, is a further important feature that often characterizes RTEs [33]. The most interesting examples of IET-PDFs are given by an exponential, indicating a Poisson process, stretched exponential and power-law decays:

$$\psi(\tau) \sim e^{-r_p \tau}; e^{-(r_p \tau)^\alpha}; \frac{1}{\tau^\mu}$$

with $0 < \alpha < 1$ and $1 < \mu < 3$. While the Poisson process is associated with the lack of self-organization, the last two behaviors, in particular the power-law, identify important non-Poisson processes marking the intermittent emergence of self-organized states [18].

In IDC systems, the testing of the renewal condition and the IET-PDF shape can be exploited to define the level of complexity [18, 29]. Inverse power-law decay in the IET-PDF represents the most interesting case, as it links to self-similarity spanning over a wide range of time scales. In this case, the power exponent μ is defined as the IDC index, thus being associated with the capacity of the cooperative dynamics to trigger self-organized metastable states [18]. Some prototypical models of signals with complex intermittency are given by the Pomeau-Manneville map, where the presence of a marginally stable point determines a sequence of fast transitions between a laminar and a chaotic region, [34, 35, 36], and by heteroclinic channels [21, 22, 37], that is, a sequence of fast passages through several saddle points that define the fast transitions between two different regions of the state space.

Event-based or intermittency-based approaches, i.e., based on the detection and sta-

tistical characterization of RTEs, were extensively applied in several fields. A greatly interesting case is given by brain dynamics, which are probably the most important prototype of a complex system [23, 8, 9, 10]. In brain studies, the authors of Refs. [19, 20] firstly introduced the idea of RTE¹ in the neuroscience field and applied to the processing of ElectroEncephaloGrams (EEGs) and MagnetoEncephaloGrams (MEG). Other authors applied similar event-based approaches and similar RTE definitions to investigate brain complexity [29, 30] functional Magnetic Resonance Imaging (fMRI) data [31, 32], neural dynamics [24, 38, 39]. The concept of RTE was also applied in several other research contexts and to different kinds of data, e.g., atmospheric turbulence [40]. In general, many different RTE definitions were exploited including, more in general, the definition of crucial transition events not directly linked to rapid passages but, e.g., to some threshold passage in the signal, often after proper processing of the signal itself [40].

The event-based approach is a basic building block of the TC/IDC framework, such as the RTE definition and the associated event detection algorithm. In this respect, the effect of noise and the presence of false positives in the event detection are unavoidable. However, in complex systems theory, the main interest lies in the reliable estimation of the system's complexity. Regarding the IDC class of complex systems, the proper evaluation of complexity indices can be affected by the goodness of the event detection algorithm, whose accuracy can be affected by noise and by the unavoidable presence of false positives. In particular, the presence of noisy, secondary, events has a blurring effect on the WT-PDF [30, 27], thereby foreclosing the possibility of a reliable estimate of the IDC index μ and, in general, or other

¹These authors actually named Rapid Transition Processes (RTPs) the here introduced concept of RTEs.

properties related to the IET-PDF and to event sequence. However, a method to treat with noisy or secondary events is the Event Driven Diffusion Scaling (EDDiS) algorithm [18, 27, 29], a method that is based on the concept of anomalous diffusion and on related well-known results found in classical literature [41, 42, 43, 44, 45, 46, 47, 48, 49, 50, 51]. This algorithm is based on the idea that secondary events drive a normal diffusion process while crucial complex events trigger anomalous diffusion [18, 52, 41, 53, 54], this last one being defined by a non-Gaussian distribution and/or a nonlinear growth of the variance²:

$$\langle X(t)^2 \rangle \sim t^{2H} .$$

H is the second-moment scaling, which corresponds to the Hurst exponent for mono-scaling signals. EDDiS algorithm is based on well-known theoretical results about diffusion processes driven by crucial events, in particular referring to the Continuous Time Random Walk (CTRW) model [52, 43, 44, 55, 56, 57]. In particular, these theoretical results follow from the assumption of the renewal condition introduced above [33].

Even if the problem of noisy events in complexity evaluation was identified and the potentiality of EDDiS was investigated [27, 29, 30], a systematic evaluation of the accuracy in the complexity estimation is still lacking.

In this paper, we carry out a systematic study of estimation errors in complexity indices derived from the EDDiS algorithm. In particular, we investigate the role of the event detection algorithm and characterize the robustness of complexity estimation concerning the choice of parameters that need to be fixed *a priori* in the

²Here $X(t)$ is the integral of an observed signal $S(t)$, i.e., $\dot{X}(t) = S(t)$.

event detection algorithm. To carry out this study we here propose and develop an extension of an event detection algorithm first proposed in Ref. Kaplan et al. [20]. Our approach is essentially a generalization of that algorithm and of later variations proposed and applied by Allegrini et al. [29, 58]. The proposed algorithm of event detection is then applied to a time series generated by a stochastic model that combines a sequence of complex events with a damped oscillator and an additive white Gaussian noise component.

The paper is organized as follows. In Section 2 we introduce the event detection algorithm, hereafter referred to as RTE Finder (RTEF), we briefly recall the EDDiS tool and we define the metrics used to evaluate the estimation errors. In Section 3 we introduce our stochastic model used to generate artificial signal driven by events with IET distributed according to an inverse power-law with a power exponent μ (complex events) or to an exponential (Poisson events). In Section 4 we illustrate the results of numerical simulations and, in particular, the application of the RTEF-EDDiS pipeline of statistical analyses to the simulated event-driven signals. In subsection 5 we give a detailed discussion of the results. Finally, in Section 6 we discuss our findings.

2. Methods of Data Analysis

Our goal is to test the accuracy in the estimation of IDC index μ by the combined applications of an event detection algorithm, herein denoted as RTE-Finder (RTEF), and of the EDDiS algorithm.

2.1. The RTEF algorithm

Our proposed algorithm is inspired by and generalizes the work of Kaplan et al. [20] and of Allegrini et al. [29, 58]. The main differences lie in the evaluation of the signal steepness, of the signal envelope and on the possibility of extending the analysis to different signal frequency bands.

The RTEF algorithm consists of two main steps: (1) calculation of the signal envelope and (2) extraction of the RTEs. In the first step, we estimate the signal envelope by using the modulus of the analytical signal associated with the Hilbert transform \mathcal{H} , i.e.:

$$S_a(t) = S(t) + i \mathcal{H}[S](t)$$

so that the envelope is given by $E(t) = |S_a(t)|$. Following the convention by Kaplan et al. [20], the signal envelope $E(t)$ is hereafter denoted as “Test Signal”. In the second step, we start from the Test Signal and calculate the approximation of its derivative to see the rapid changes in the signal. The derivative of the Test Signal at time t_k is estimated by the following formula:

$$\dot{E}(t_k) = \frac{1}{N_d} \sum_{j=1}^{N_d} \frac{E(t_k + jT_s) - E(t_k - jT_s)}{2 \cdot j \cdot T_s} \quad (1)$$

being N_d the time window that we consider to estimate the derivative and T_s the sampling time of the signal. Eq. (1) is an average of N_d difference quotients, centered at t_k , taken at different time intervals $2 \cdot j \cdot T_s$ around t_k itself. For the estimation

of the derivative we considered two time windows: $N_d = 5$ and $N_d = 12$. We only report here the results obtained with $N_d = 5$, while the analyses carried out with $N_d = 12$ can be found in the Supplementary Material.

Finally, we compute the absolute value of the derivative and we determine a threshold by selecting a specific percentile value from the distribution of these absolute values. The RTEs are then defined by the threshold crossings of the absolute value of the derivative.

2.2. EDDiS Algorithm

The EDDiS method is a combination of two scaling analyses applied to three different random walks driven by a sequence of events. We here limit to the application of one particular random walk, based on the Asymmetric Jump (AJ) rule, and recall the two scaling analyses carried out on the resulting diffusion process. Further details of the EDDiS algorithm can be found in Refs. [18, 27, 29] and, for reader's convenience, in the Supplementary Material.

The two scaling analyses are given by the Diffusion Entropy [41, 53, 54], which evaluate the similarity δ of the diffusion PDF, and by the Detrended Fluctuation Analysis (DFA) [59], estimating the second moment scaling H , essentially corresponding to the so-called Hurst exponent [60]. The scaling exponent H of the second moment is defined as:

$$\sigma^2(t) = \langle (X(t) - \bar{X}(t))^2 \rangle \sim t^{2H} \quad (2)$$

being $X(t)$ the diffusion variable resulted after applying the walking rule, and $\bar{X}(t)$ is a proper local trend of $X(t)$. The self-similarity index δ is defined as:

$$P(x, t) = \frac{1}{t^\delta} F\left(\frac{x}{t^\delta}\right) \quad (3)$$

being $P(x, t)$ the PDF of the diffusion variable $X(t)$.

In general, the diffusion variable is written as the integral of a temporal signal:

$$X(t) = \int_0^t \xi(t') dt' \approx \sum_{n=0}^N \xi_n$$

being $t = t_N$. In the AJ walking rule here applied, the impulsive, time-sampled, variable ξ_n consists of making a unitary jump ahead when an event occurs. The resulting event-driven diffusion process built according to the AJ rule corresponds to the counting process generated by the event sequence:

$$X(t) = \#\{n : t_n < t\}. \quad (4)$$

The functional relationships $\delta = \delta(\mu)$ and $H = H(\mu)$ in the case of AJ are the following [18, 41]:

$$H_{AJ} = \begin{cases} \frac{\mu}{2} & \text{if } 1 < \mu < 2 \\ 2 - \frac{\mu}{2} & \text{if } 2 \leq \mu < 3 \\ \frac{1}{2} & \text{if } \mu \geq 3 \end{cases} \quad (5)$$

$$\delta_{AJ} = \begin{cases} \mu - 1 & \text{if } 1 < \mu < 2 \\ \frac{1}{\mu-1} & \text{if } 2 \leq \mu < 3 \\ \frac{1}{2} & \text{if } \mu \geq 3 \end{cases} \quad (6)$$

For this study, we apply this method directly to the detected RTE sequences. This type of analysis is a powerful tool for scaling detection and, under the assumption of superdiffusion, i.e., $H > 0.5$ and of sufficiently long sequence of events, is effective in detecting the anomalous diffusion scaling, thus giving useful information on the underlying dynamics that indeed generate the events. In the following, H , δ and μ will be generically referred to as *complexity indices*.

2.3. Error estimates

To have a metric of performances of the proposed algorithm, we calculate the relative error for different metrics:

$$RE = \left| \frac{EV - RV}{RV} \right| \quad (7)$$

where EV is the estimated value, and RV is the real value. When the RE is referred to a set of numerical simulations, we compute the average of the RE over these same simulations and denote it as Mean RE (MRE).

3. The time series model

The model used to simulate the time series, or temporal signals, is inspired to the work of Guardabasso et al. [61]. In particular, Guardabasso and co-workers studied a noisy relaxation process triggered by a sequence of random events with Poisson statistics. We introduce here an extension of their model by introducing two elements:

- A Non-Poisson distribution of events according to a IET-PDF with inverse power-law decay³.
- A damped oscillator that is triggered by each event and whose dynamics are modeled through a second-order differential equation.

Similarly to Guardabasso et al. [61], a Gaussian white noise component is then added to the synthetic time series.

In summary, the time series model is divided into four main steps:

³The analysis of complex events, associated with an inverse power-law IET-PDF, is here compared with the standard Poisson events investigated by Guardabasso et al. [61].

- (a) Generation of an event sequence, described by the corresponding set of event occurrence times: $\{t_n; 1 \leq n \leq M\}$.
- (b) Generation of a pulse amplitude A_n for each event, with A_n uniform random number in $[1, 10]$. At this point, we get a train of pulses with different amplitudes and the point process is described by the set $\{(t_n, A_n); 1 \leq n \leq M\}$ and by the formula:
- $$S_{PT}(t) = \sum_{i=0}^M A_i \delta(t - t_i) \quad (8)$$
- (c) Convolution with pulse response: for each event, this step generates a damped oscillation, which then generalizes the relaxation process of Guardabasso et al. [61].
- (d) Addition of Gaussian white noise to the generated time series.

In step (a) a sequence of IETs, also known as Waiting Times (WTs), is first drawn from a given IET-PDF. In particular, we choose two types of probability distributions [18]:

- Inverse power-law distribution for complex events [27, 41, 54]:

$$\psi_n(\tau) = \frac{\mu - 1}{T} \frac{1}{(T + \tau)^\mu} \quad (9)$$

being μ the power-law exponent and T the time scale at which the power law emerges⁴.

- Exponential distribution for Poisson events

$$\psi_p(\tau) = r_p e^{-r_p \tau} \quad (10)$$

⁴When $\mu > 2$, the mean IET is given by $\langle \tau_n \rangle = T/(\mu - 2)$.

where r_p is the Poisson's event rate and $\langle \tau_p \rangle = 1/r_p$.

For both cases we set the mean IET equal to 1 ($\langle \tau_p \rangle = \langle \tau_n \rangle = 1$) and we draw a sample of $M = 20000$ IETs to get a sequence of random events. In the case of power-law distribution, we draw the IETs by using the following formula [62]:

$$\tau_i = T \left(\xi_i^{\frac{1}{1-\mu}} - 1 \right) ; i = 0, 1, \dots \quad (11)$$

being ξ_i a random number uniformly distributed in $[0, 1]^5$.

The IETs from the exponential distribution are drawn using the usual expression:

$$\tau_i = -\frac{1}{r_p} \log \xi_i ; i = 0, 1, \dots \quad (12)$$

where, as in Eq.(11), ξ_i is a random number uniformly distributed in $[0, 1]$. In Figure 1 some generated IET-PDFs are reported together with the related theoretical curves, making it evident that the qualitative comparison is very good. Then, the sequence of event occurrence times is simply defined by:

$$t_n = t_{n-1} + \tau_n ; t_0 = 0 ; n = 1, 2, \dots, M$$

The total simulation time is given by $t_{max} = t_M$. In order to reproduce a sampled signal, we then established a sampling grid spanning from 0 to t_{max} with a sampling time $T_s = 0.01^6$. Starting from Eq. (8), the discrete time version of the pulse train is given as a sequence of zeros at each time step except for the steps that are nearer to an event occurrence time. In formulas, given $t_i = i \cdot T_s$ with t_i the time step that is nearest to the event occurrence time t_n , it results: $S_{pT}(t_i) = A_n$. Subsequently, according to above point (c), we generated a time series based on the pulse train using the following algorithm:

⁵This formula is also obtained by applying the cumulative function method.

⁶When considering time units in seconds, this corresponds to a sampling rate of 100Hz.

1. Take an angular frequency band: $[\omega_{0_{min}}, \omega_{0_{max}}]$, or equivalently, a frequency band: $[\nu_{min}, \nu_{max}]$, being that $\omega = 2\pi\nu$.
2. Choose N angular frequencies ω_{0_k} equispaced in the band. In our case the grid size $\Delta\omega_0 = 1$.
3. For each ω_{0_k} the pulse response function is given by a damped oscillator:

$$I_k(t) = \frac{e^{-\frac{\gamma}{2}t}}{\omega_{1_k}} \sin(\omega_{1_k} t) \quad (13)$$

where $\omega_{1_k} = \frac{1}{2}\sqrt{4\omega_{0_k}^2 - \gamma^2}$, and γ is the relaxation factor of the damped oscillator. Notice that this is the solution of a second-order differential equation representing the dynamics of a particle in a harmonic potential with friction, i.e.:

$$\frac{dI_k}{dt} = v_k ; \quad \frac{dv_k}{dt} = -\gamma v_k - \omega_{0_k}^2 x_k + \delta(t) \quad (14)$$

being $I_k(0) = 0$, $v_k(0) = 1$ ⁷. The Dirac function $\delta(t)$ in Eq. (14) is a pulse at time $t = 0$ and the solution to this equation, given in Eq. (13), is the fundamental solution (Green function) of the system of differential equations in Eq. (14) and, thus, the response to this initial pulse.

4. Then, for each event occurrence time t_n , the total pulse response function is given by the superposition of all contributions in the frequency band:

$$I(t) = \sum_{k=1}^N I_k(t) = \sum_{k=1}^N \frac{e^{-\frac{\gamma}{2}t}}{\omega_{1_k}} \sin(\omega_{1_k} t) \quad (15)$$

5. The total generated time series is then given by the time convolution between $I(t)$ and $S_{PT}(t)$:

$$S(t) = (I * S_{PT})(t)$$

⁷The response function (13) is also referred to as a second-order linear filter.

The sampled signal $S(T_i) = S(i)$ ⁸ is calculated by Z-transforming the function $I(t)$ and by multiplying it with the Z-transform of the pulse train $S_{PT}(t)$. At the end of this step, given the sampling time T_s and the time steps $t_i = i \cdot T_s$, we get a sampled signal $S(i)$ by anti-transforming.

6. A Gaussian noise $W(t)$ is added to the time series, that is, a sequence of Gaussian random variables $W(i)$. The Gaussian noise has zero mean and variance computed as a fraction of the variance computed from the time series obtained in the previous step. In formulas:

$$S(i) = \mathcal{Z}^{-1} [\mathcal{Z} [S_{PT}] \mathcal{Z} [I]] (i) + W(i) ; \quad 0 \leq i \cdot T_s \leq t_{max} = t_M \quad (16)$$

The algorithm's functionality is illustrated in Figure 2, the noise variance is set to 10% of the variance computed from the time series without noise.

We evaluate the performance of the RTEF by generating time series in three distinct frequency bands $[\nu_{min}, \nu_{max}]$: $[0.5, 4]$ Hz, $[4, 8]$ Hz, and $[8, 12]$ Hz. Figure 3 shows an example of the same time series generated in these different frequency bands starting from the same event sequence, without noise.

⁸Since there are no ambiguities, it is possible to use the concise notation $S(i)$ for the sample signal.

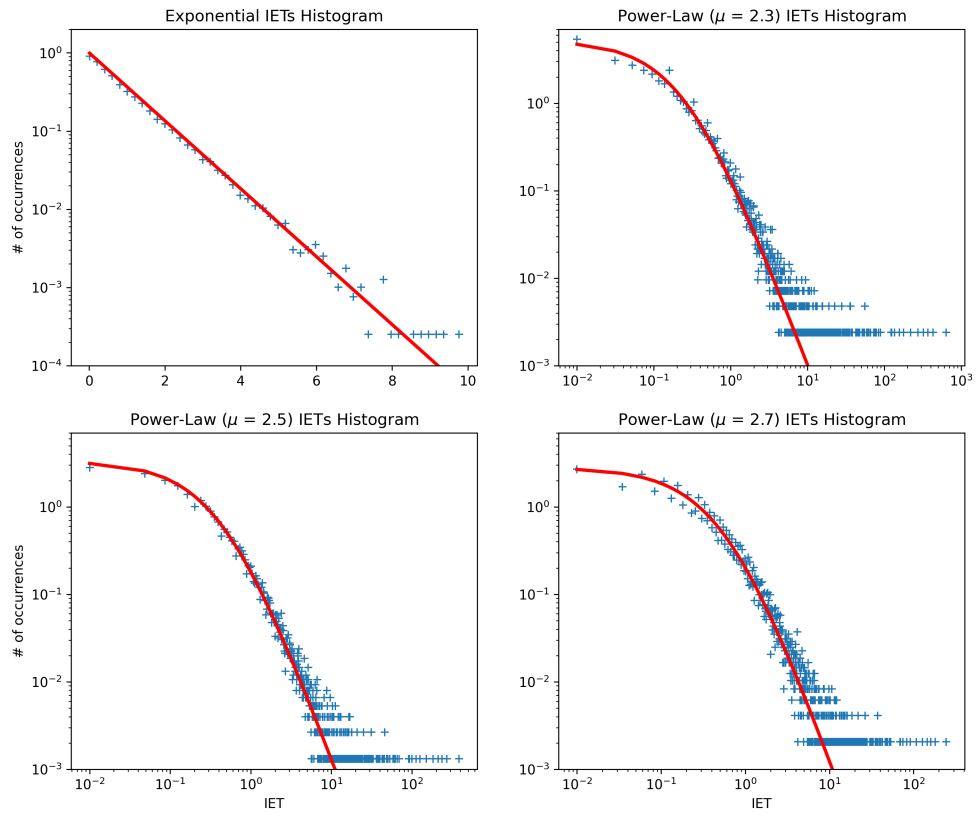


Figure 1: Comparison of observed IET distributions with theoretical curves.

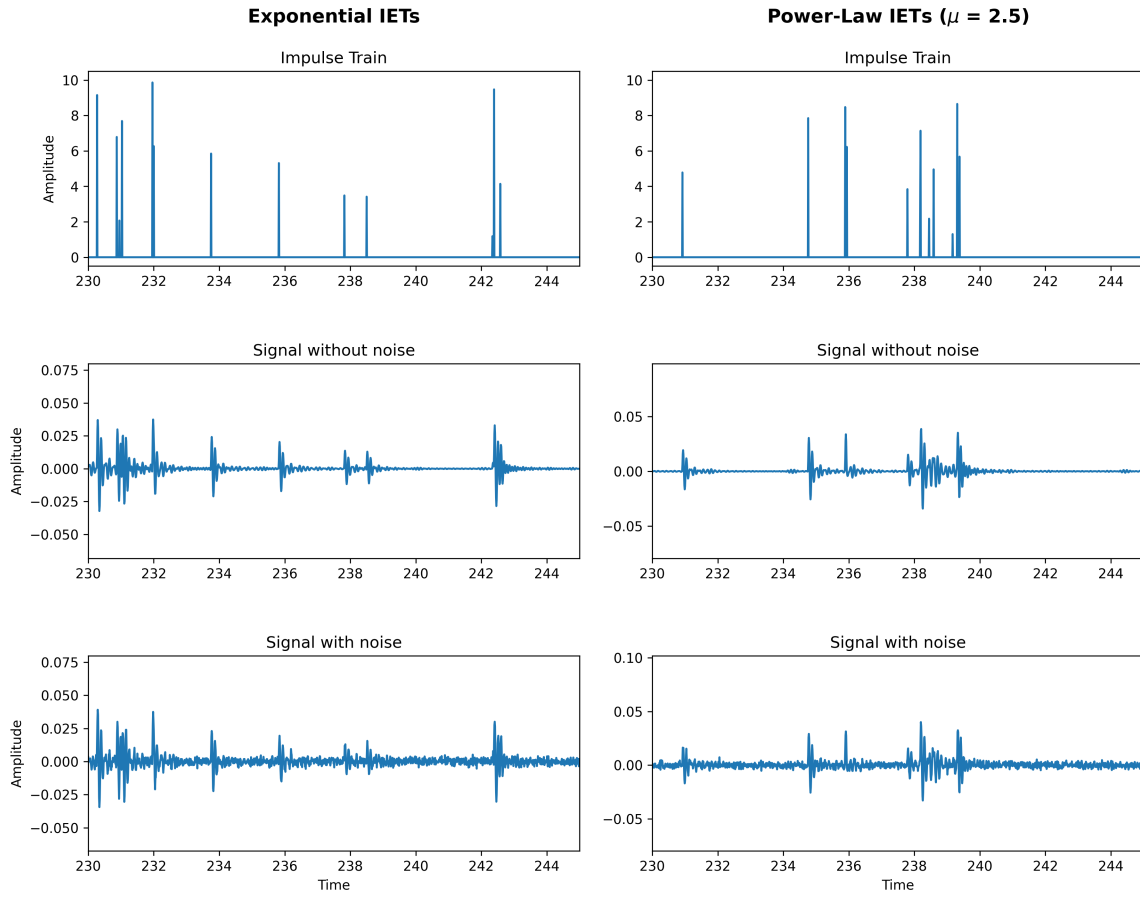


Figure 2: Example of time series generated by our model. Left and right panel refer to exponential and power-law (with $\mu = 2.5$) IET distributions, respectively. Top: comparison of the impulse trains. Middle: time series generated without the noise in frequency band $[8, 12]Hz$. Bottom: final time series with noise (with 10% variance of the deterministic component).

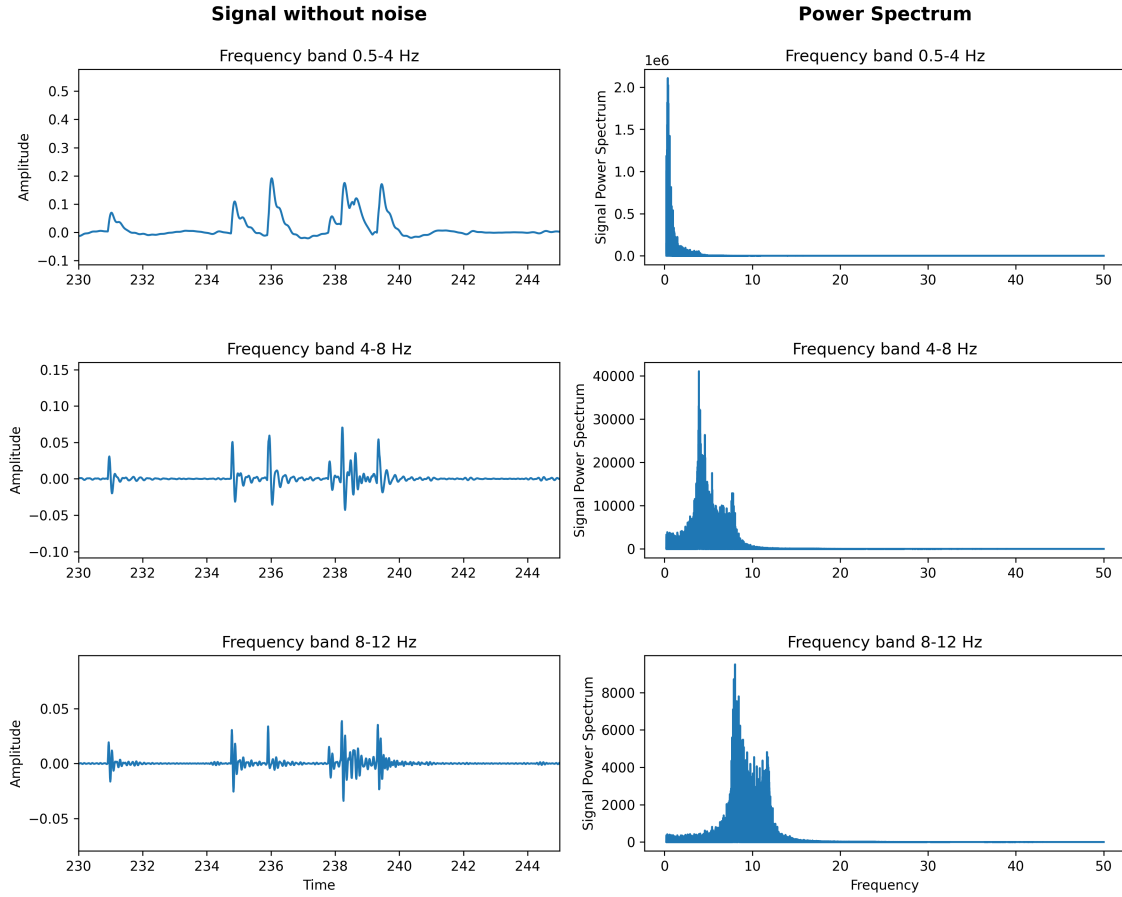


Figure 3: Example of a time series generated in different frequency bands. Left panels: generated time series; same event sequence as in the top right panel of Figure 2 (power-law, $\mu = 2.5$). Right panels: power spectra corresponding to the time series reported in the left panels.

4. Numerical Simulations and Results

To test the RTEF algorithm we simulated different synthetic time series exploiting the model introduced in the previous Section 3. We generated a total of 150 signals for each IET-PDF, which are: power-law with $\mu = 2.3$, $\mu = 2.5$, $\mu = 2.7$; exponential with $r_p = 1$. We recall that all IET sequences are constrained to a unitary mean IET.

This is immediate in the exponential case, being $\langle \tau_p \rangle = 1/r_p = 1$. Conversely, in the power-law case, the parameter T in Eqs. (9) and (11) must obey the relationship: $T/(\mu - 2) = \langle \tau_n \rangle = 1$.

For each IET-PDF, 50 different sample sets of IETs were drawn: $\{\tau_n; n = 1, M\}$ ($M = 20000$). The associated sequence of event time occurrence is then given by: $t_0 = 0, t_n = t_{n-1} + \tau_n, n \geq 1$. For each sample set of IET, we apply the points (4-5) of the algorithm for three different frequency bands of the signal: $[0.5, 4]$ Hz, $[4, 8]$ Hz, and $[8, 12]$ Hz. We finally add the Gaussian noise, as described in the point (6) of the previous section, to get the final temporal signal.

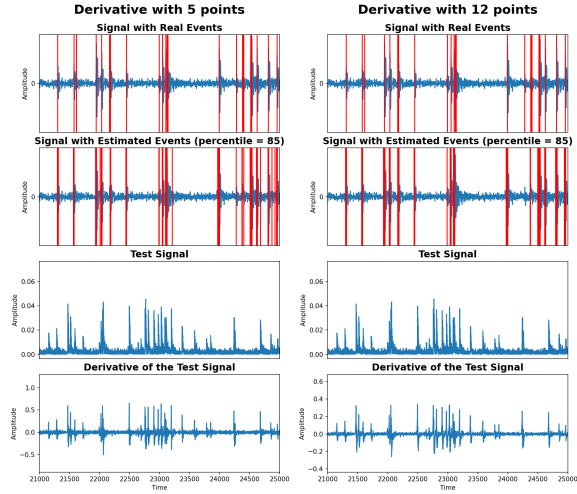
We first evaluated the complexity indices H and δ directly on the IET samples, giving an estimation of relative errors due only to the random drawing, that is, to the random number generator, and to the best fit algorithm. This is obtained by applying the EDDiS, limited to the AJ walking rule, to the IET samples. These estimated relative errors, which will be denoted in the following as *reference errors*, are presented in Table 1. This is a useful estimation of the statistical error associated with the random generator and the best fit procedure that can be used as a set of reference values for the combined RTEF-EDDiS pipeline.

As illustrated before, we used two different time windows to estimate the derivative of the envelope of the absolute value of the signal. In Figure 4 we display an example of how the RTEF algorithm works. In particular, these panels highlight that there are important differences in choosing $N_d = 5$ or $N_d = 12$ symmetrical points to estimate the derivative. In fact, for all the percentile values that we used, the estimation of the derivative with $N_d = 5$ gives more precise results than the one with $N_d = 12$. Moreover, by passing from the 85th to the 98th percentiles, the number of false positives decreased, but some real events were missed. In Figure 4 we report only

the results with the 85th and the 98th percentiles, whereas other results with 90th and 95th percentiles are reported in the Supplementary Material. The IET distribution of the real and of the detected RTEs are similar but with some differences. In Figure 5 we can see that there are some differences in the IET-PDFs estimated by using 5 or 12 symmetrical points to estimate the derivative. The estimated distributions by using 5 symmetrical points are more similar to the real one with respect to the one estimated with 12 symmetrical points. By passing from the 85th percentile to the 98th percentile we noticed that the exponential distribution and the initial part of the power-law distributions got worse, while the tails of the power-law distributions became more similar to the real one. Even if not trivial, this result is expected by observing that a higher percentile value select time events with greater signal steepness. However, it is worth noting that the estimations of the IET distributions are quite robust concerning the change in both N_d and percentile.

To estimate the diffusion scaling parameter derived from the detected events, we employed the DFA and DE analyses. In Figure 6 and Figure 7, we report the average results of the DFA and DE analysis with error bars and with all the percentile values chosen. We report here the results obtained for signals generated in the frequency band $[8, 12]$ Hz, while the results obtained for signals generated in frequency bands $[0.5, 4]$ Hz and $[4, 8]$ Hz are reported in the Supplementary Materials. Tables 2, 3, 4, and 5 present the Mean Relative Errors (MREs) with Standard Deviations (STDs) of estimated scaling parameters H and δ obtained for each percentile and each frequency band, limited to $N_d = 5$. We chose to report only the 5-point results due to their better performance compared to the 12-point results, which are included in the Supplementary Material.

(a) 85th Percentile



(b) 98th Percentile

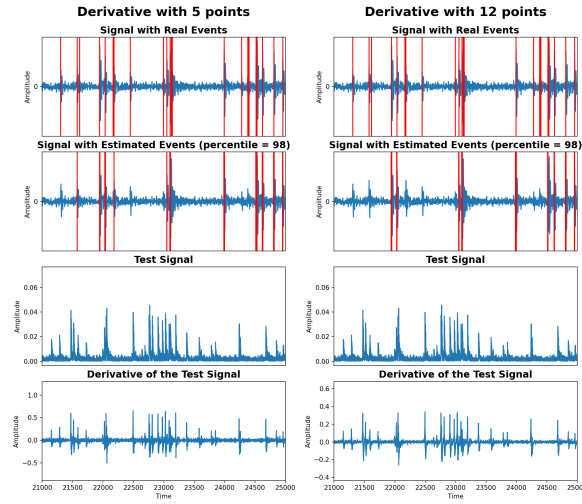


Figure 4: Example of application of the RTEF algorithm. The results are obtained using 5 or 12 symmetrical points to estimate the derivative for a signal generated in frequency band $[8, 12]$ Hz. On the first two top panels, vertical red lines indicate the real (above) or estimated (below) events. (a) RTEF results for the 85th percentile of the derivative distribution. (b) RTEF results for the 98th percentile of the derivative distribution.

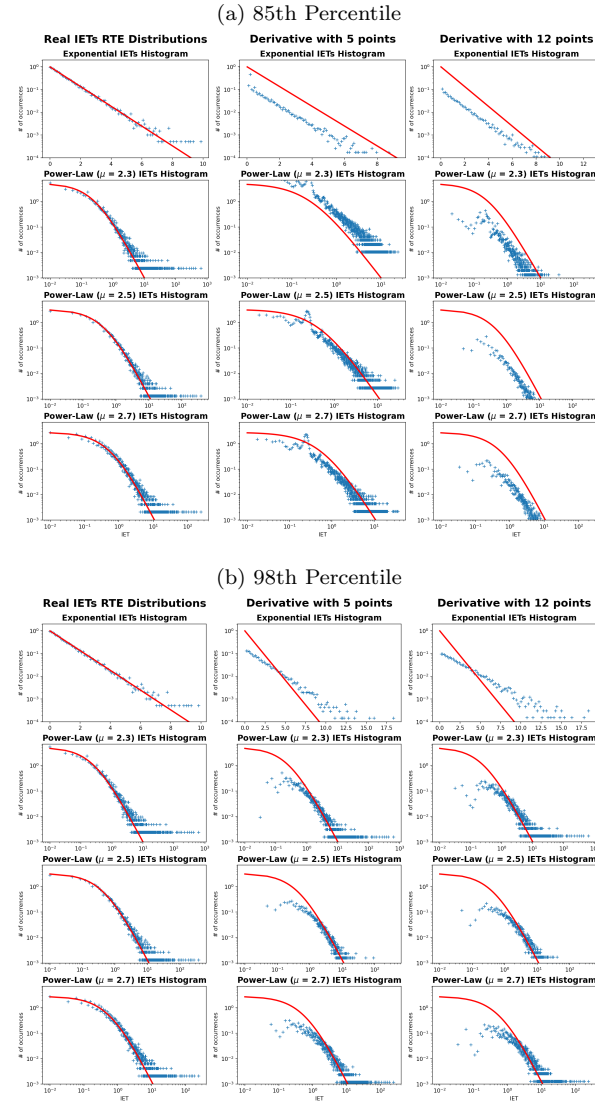


Figure 5: Comparison of real IET distributions to the estimated ones for a signal generated in frequency band $[8, 12]$ Hz and using 5 or 12 symmetrical points to estimate the derivative. The red lines represent the theoretical curves. (a) Comparison of real IETs to the estimated one from the 85th percentile of the derivative distribution. (b) Comparison of real IETs to the estimated one from the 98th percentile of the derivative distribution.

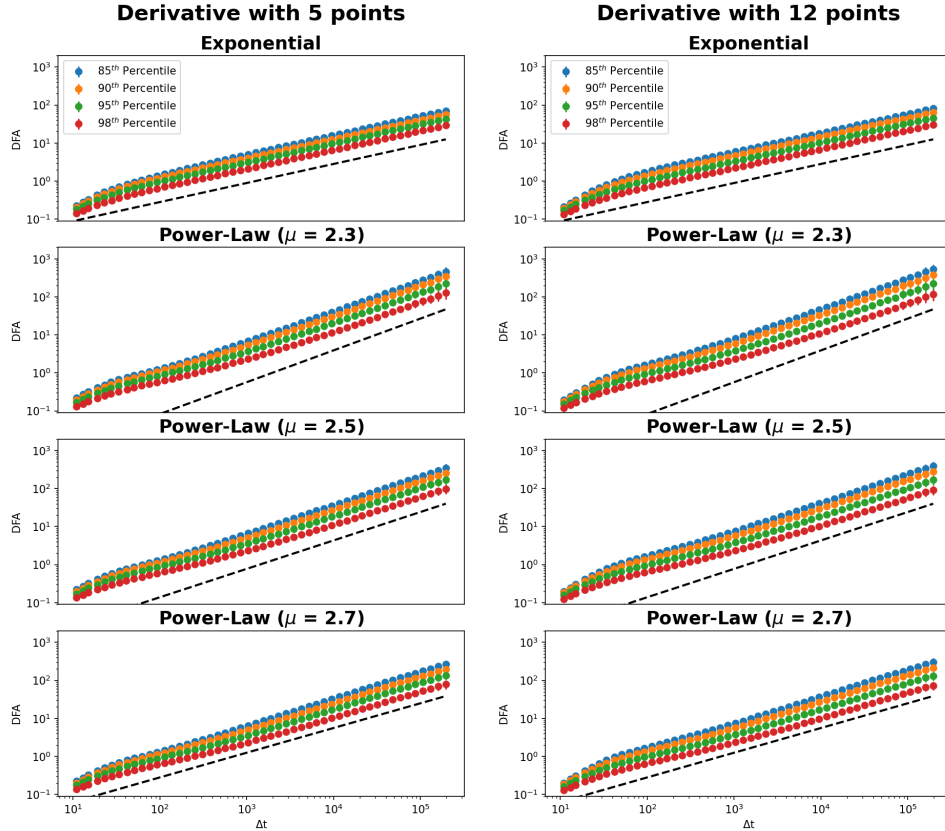


Figure 6: DFA mean curves with error bars for signals generated in frequency band $[8, 12]$ Hz. Mean and error bars are computed over the 50 IET samples. This figure compares the DFA curves obtained using $N_d = 5$ and $N_d = 12$ symmetrical points to estimate the derivative. The dashed black lines represent the theoretical slope, that is: $H = 0.5$ for the Exponential Distribution, $H = 0.85$ for Power-Law distribution with $\mu = 2.3$, $H = 0.75$ for $\mu = 2.5$, and $H = 0.65$ for $\mu = 2.7$.

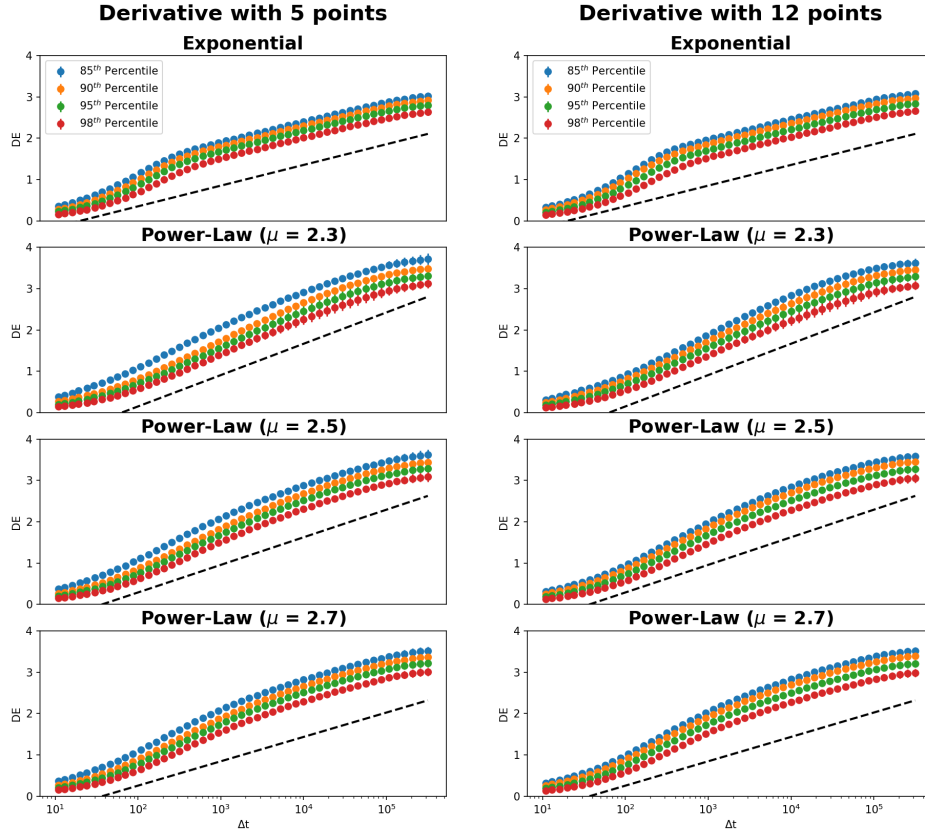


Figure 7: DE mean curves with error bars for signals generated in frequency band $[8, 12]$ Hz. Mean and error bars are computed over the 50 IET samples. This figure compares the DE curves obtained using $N_d = 5$ and $N_d = 12$ symmetrical points to estimate the derivative. The dashed black lines represent the theoretical slope that is: $\delta = 0.5$ for the Exponential Distribution, $\delta \simeq 0.77$ for Power-Law distribution with $\mu = 2.3$, $\delta \simeq 0.67$ for $\mu = 2.5$, and $\delta \sim 0.59$ for $\mu = 2.7$.

Case	MRE H (\pm STD)	MRE δ (\pm STD)
Exponential	0.0052 (\pm 0.0042)	0.024 (\pm 0.011)
Power-Law ($\mu = 2.3$)	0.088 (\pm 0.040)	0.040 (\pm 0.035)
Power-Law ($\mu = 2.5$)	0.040 (\pm 0.030)	0.062 (\pm 0.021)
Power-Law ($\mu = 2.7$)	0.070 (\pm 0.040)	0.15 (\pm 0.030)

(a) DFA and DE Mean Relative Errors

Case	MRE μ or r_p (\pm STD)	Min and Max Relative Error
Exponential	0.019 (\pm 0.012)	[0.001, 0.044]
Power-Law ($\mu = 2.3$)	0.068 (\pm 0.055)	[0.0031, 0.25]
Power-Law ($\mu = 2.5$)	0.061 (\pm 0.046)	[0.0002, 0.22]
Power-Law ($\mu = 2.7$)	0.051 (\pm 0.041)	[0.0015, 0.16]

(b) Fit Mean Relative Errors

Table 1: *Reference errors* for complexity analysis carried out directly on the IET samples (average and standard deviation are computed on the 50 IET samples). (a) Mean Relative Errors (MREs) with Standard Deviation (STD) of DFA and DE; (b) MREs and STDs on μ for Power-Law and r_p for exponential distributions computed on the 50 IET samples.

Frequency Band	Percentile	MRE H (\pm STD)	MRE δ (\pm STD)
[0.5, 4]	85	0.033 (\pm 0.016)	0.056 (\pm 0.050)
	90	0.038 (\pm 0.017)	0.061 (\pm 0.051)
	95	0.037 (\pm 0.016)	0.081 (\pm 0.065)
	98	0.033 (\pm 0.018)	0.12 (\pm 0.084)
[4, 8]	85	0.031 (\pm 0.015)	0.073 (\pm 0.052)
	90	0.014 (\pm 0.010)	0.082 (\pm 0.054)
	95	0.010 (\pm 0.010)	0.085 (\pm 0.064)
	98	0.012 (\pm 0.010)	0.11 (\pm 0.083)
[8, 12]	85	0.028 (\pm 0.015)	0.069 (\pm 0.052)
	90	0.013 (\pm 0.010)	0.072 (\pm 0.048)
	95	0.010 (\pm 0.010)	0.080 (\pm 0.054)
	98	0.012 (\pm 0.010)	0.091 (\pm 0.069)

Table 2: MREs and STDs of DFA and DE computed from detected events in signals driven by exponential IET distributions (MREs and STDs computed from the 50 IET samples). All parameter configurations of the RTEF algorithm are reported for comparison. Results were obtained by using $N_d = 5$.

Frequency Band	Percentile	MRE H (\pm STD)	MRE δ (\pm STD)
[0.5, 4]	85	0.073 (\pm 0.044)	0.060 (\pm 0.011)
	90	0.079 (\pm 0.049)	0.10 (\pm 0.013)
	95	0.10 (\pm 0.064)	0.12 (\pm 0.014)
	98	0.10 (\pm 0.052)	0.044 (\pm 0.017)
[4, 8]	85	0.065 (\pm 0.044)	0.17 (\pm 0.040)
	90	0.077 (\pm 0.050)	0.13 (\pm 0.033)
	95	0.081 (\pm 0.046)	0.090 (\pm 0.030)
	98	0.10 (\pm 0.056)	0.040 (\pm 0.024)
[8, 12]	85	0.064 (\pm 0.040)	0.17 (\pm 0.036)
	90	0.073 (\pm 0.043)	0.12 (\pm 0.034)
	95	0.077 (\pm 0.043)	0.090 (\pm 0.031)
	98	0.092 (\pm 0.050)	0.046 (\pm 0.025)

Table 3: MREs and STDs of DFA and DE computed from detected events in signals driven by Power-Law IET distribution with $\mu = 2.3$ and $T = 0.3$ (MREs and STDs computed from the 50 IET samples). All parameter configurations of the RTEF algorithm are reported for comparison. Results were obtained by using $N_d = 5$.

Frequency Band	Percentile	MRE H (\pm STD)	MRE δ (\pm STD)
[0.5, 4]	85	0.073 (\pm 0.035)	0.17 (\pm 0.055)
	90	0.080 (\pm 0.031)	0.19 (\pm 0.076)
	95	0.095 (\pm 0.036)	0.23 (\pm 0.074)
	98	0.12 (\pm 0.054)	0.19 (\pm 0.014)
[4, 8]	85	0.041 (\pm 0.014)	0.24 (\pm 0.092)
	90	0.061 (\pm 0.030)	0.28 (\pm 0.065)
	95	0.063 (\pm 0.042)	0.24 (\pm 0.044)
	98	0.071 (\pm 0.045)	0.17 (\pm 0.018)
[8, 12]	85	0.040 (\pm 0.020)	0.24 (\pm 0.092)
	90	0.052 (\pm 0.033)	0.28 (\pm 0.060)
	95	0.051 (\pm 0.033)	0.24 (\pm 0.043)
	98	0.062 (\pm 0.042)	0.18 (\pm 0.020)

Table 4: MREs and STDs of DFA and DE computed from detected events in signals driven by Power-Law IET distribution with $\mu = 2.5$ and $T = 0.5$ (MREs and STDs computed from the 50 IET samples). All parameter configurations of the RTEF algorithm are reported for comparison. Results were obtained by using $N_d = 5$.

Frequency Band	Percentile	MRE H (\pm STD)	MRE δ (\pm STD)
[0.5, 4]	85	0.020 (\pm 0.010)	0.14 (\pm 0.098)
	90	0.023 (\pm 0.014)	0.13 (\pm 0.090)
	95	0.018 (\pm 0.013)	0.18 (\pm 0.10)
	98	0.051 (\pm 0.018)	0.25 (\pm 0.088)
[4, 8]	85	0.071 (\pm 0.021)	0.16 (\pm 0.090)
	90	0.029 (\pm 0.015)	0.23 (\pm 0.11)
	95	0.028 (\pm 0.011)	0.23 (\pm 0.11)
	98	0.055 (\pm 0.030)	0.24 (\pm 0.087)
[8, 12]	85	0.066 (\pm 0.015)	0.17 (\pm 0.095)
	90	0.024 (\pm 0.012)	0.23 (\pm 0.011)
	95	0.030 (\pm 0.010)	0.23 (\pm 0.011)
	98	0.049 (\pm 0.027)	0.23 (\pm 0.095)

Table 5: MREs and STDs of DFA and DE computed from detected events in signals driven by Power-Law IET distribution with $\mu = 2.7$ and $T = 0.7$ (MREs and STDs computed from the 50 IET samples). All parameter configurations of the RTEF algorithm are reported for comparison. Results were obtained by using $N_d = 5$.

5. Discussion of results

We here give a detailed discussion of the numerical results regarding the application of EDDiS algorithm to the IET samples and of the RTEF-EDDiS pipeline to the artificial signals driven by the same IET samples.

5.1. EDDiS analysis of IET samples and reference errors

Reference errors are due to: finite size of the statistical sample; limitations of the random number generator; and intrinsic errors of the best-fit procedure. These

errors were estimated by applying the EDDiS algorithm to the IET samples. The ideal values of H , δ and μ are given by Eqs. (5) and (6) and are compared to the corresponding estimated values by applying the RE formula, Eq. (7), and taking the average over the 50 samples to get the MRE.

Table 1a shows the mean relative errors in the estimation of the scaling factors H and δ obtained by applying DFA and DE algorithms on the real events drawn from all considered IET-PDFs. Notably, the relative errors for both scaling factors across all IET distributions remain below 10%, except for the δ scaling factor estimated for the inverse power-law distribution with $\mu = 2.7$, which reaches 15%. In particular, the estimated H values consistently exhibited a relative error below 8.8%, with the lowest error occurring for the exponential distribution and the highest for the power-law distribution with $\mu = 2.3$. Conversely, the δ estimated values have higher MRE than H values, reaching a maximum of 15% for the power-law distribution with $\mu = 2.7$. There is only one exception: the power-law distribution with $\mu = 2.3$, where the relative error of δ was lower than that of H (4.0% compared to 8.8%).

Table 1b highlights that the mean relative errors in the direct μ (or r_p) evaluation, i.e., from the fit of IET-PDFs, for all the cases do not pass the 7% on average. As expected, the best performance is given by the evaluation of r_p in the exponential case, while the accuracy in μ evaluation increases (MRE decreases) as μ increases, thus giving the worst performance for the slower power-law decay, i.e., $\mu = 2.3$. Moreover, an analysis of the confidence intervals revealed a maximum relative error of 25% in the worst-case scenario and of 0.44% in the best-case scenario. In contrast, the minimum relative errors were assessed at 0.31% in the worst-case scenario and 0.02% in the best-case scenario.

In general, the δ and H evaluations have the highest accuracy for the exponential case. For the power-law case, δ is better estimated for smaller μ , while the accuracy

of H estimation is not monotonic with μ , giving the best result for $\mu = 2.5$ (4%).

5.2. RTEF-EDDiS analysis of event-driven artificial signals

The artificial signals generated according to the model of Section 3 were processed with the RTEF algorithm and the detected events were exploited to estimate the scaling exponents H and δ through the EDDiS algorithm. We found that the RTEF algorithm’s performance is primarily affected by the number N_d of symmetrical time points used for derivative estimation of the absolute value of the signal’s envelope. In particular, we highlight that the case $N_d = 5$ generally outperforms the case $N_d = 12$. For this reason, we here focus the discussion on the case $N_d = 5$, while interested readers can find the results obtained using $N_d = 12$ in the supplementary material. Another crucial factor affecting the RTEF-EDDiS pipeline’s performance is the percentile value used to select the RTEs. As expected, the lower the percentile value, the more false positives are found. From Figure 8 we can see that the number of detected RTEs spanned from two times to almost ten times the number of real RTEs going from 95th to 85th percentile values, thus revealing a very large number of false positives. Only the 98th percentile gives RTE counts comparable with the real number of RTEs (20000), but still with an overestimation error of about 20 – 30%.

5.2.1. Exponential case

For the exponential case, summarized in Table 2, the accuracy in H improves as the percentile increases, or remains almost constant for the band $[0.5, 4]$. This last band is also that giving the worst MREs, which however remain below 4%. At variance with H , in all bands, the accuracy in the δ evaluation decreases as the percentile increases.

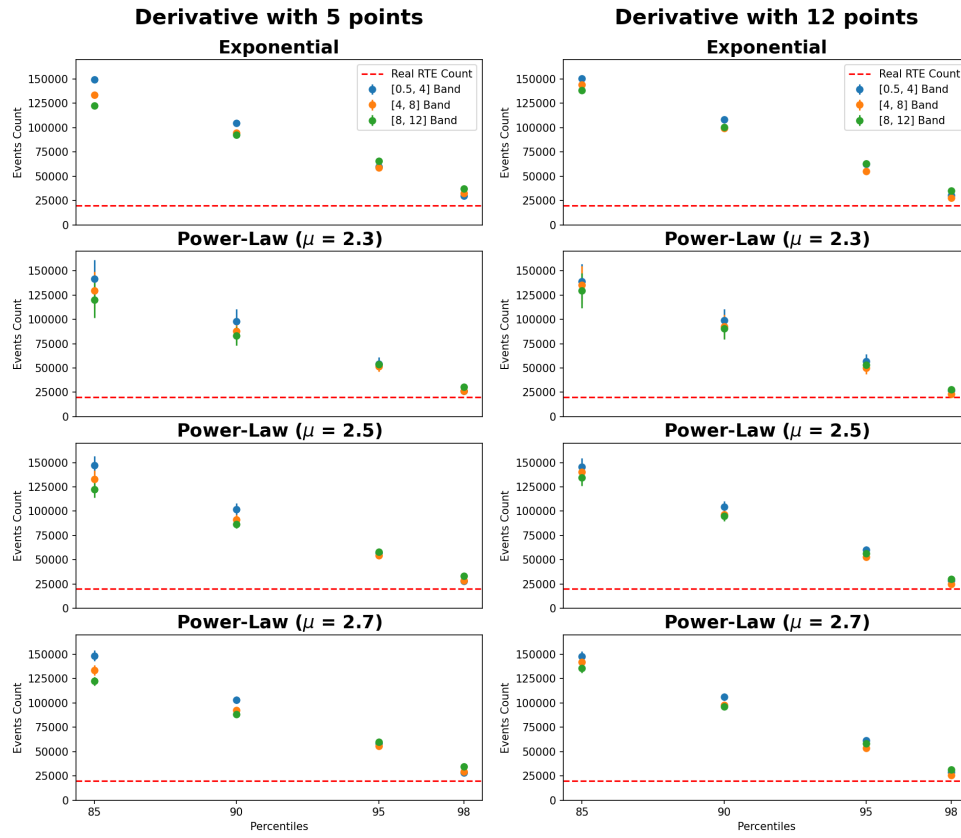


Figure 8: Mean estimated RTE counts with error bars for each IET distribution and frequency band vs percentile values. Left panels and right panels refer to $N_d = 5$ and $N_d = 12$, respectively. The dashed red lines represent the number of real RTEs that is equal to 20000.

5.2.2. Power-law $\mu = 2.3$

For the power-law distribution with $\mu = 2.3$, we find the counter-intuitive result that the relative errors of H are generally smaller than the reference errors of Table 1. Further, accuracy improves as percentile decreases, a condition corresponding to a much larger number of false positives in the RTE detection. Additionally, the variation in H relative errors between frequency bands is minimal. Conversely, the relative errors of δ are typically higher than reference errors and generally decrease as the percentile increases. In the band $[0.5, 4]$ a non-monotonic behavior is seen, but the best accuracy is still found at the 98th percentile with a 4.4% relative error. Errors in δ are slightly larger than those in H .

5.2.3. Power-law $\mu = 2.5$

For the power-law distribution with $\mu = 2.5$, we find that the relative errors of H and δ are generally higher than the reference errors. Similarly to previous cases, the differences in the relative errors between frequency bands are minimal, even if we found slightly better results for H in the $[4, 8]$ Hz and $[8, 12]$ Hz bands.

Regarding δ , the accuracy is non-monotonic with the percentile. The best results are given by the 98th percentile in the $[4, 8]$ and $[8, 12]$ bands, and by the 85th percentile in the $[0.5, 4]$ band. Interestingly, the errors in δ are much higher than those in H .

5.2.4. Power-law $\mu = 2.7$

Surprisingly, for the power-law distribution with $\mu = 2.7$, the relative errors of H are consistently lower than reference errors given in Table 1a. Conversely, the δ relative errors are generally greater or equal to the corresponding reference errors. Regarding frequency band differences, minimal variations were observed in the relative errors of both H and δ between $[4, 8]$ and $[8, 12]$ bands, while the $[0.5, 4]$ Hz band exhibits slightly better results. Finally, the 90th and 95th percentiles yielded the best results

for H estimation, while the δ estimation improves as the percentile decreases, reaching the best performance at the 85th percentile. Similarly to the case $\mu = 2.5$, the errors in δ are much higher than those in H .

6. Concluding remarks

In this work, we evaluated the effect of an event detection algorithm on the estimation accuracy of event-based complexity indices μ , H and δ . In the present study we were not interested in the efficiency of single-event detection, but in the possibility of getting a good estimation of the genuine temporal complexity. In particular, our main interest lies in the evaluation of signals driven by complex events, that is, events with inverse power-law IET distributions.

In Table 6 we summarize the best and worst relative errors for H and δ compared to the corresponding reference errors, while in Figs. 9 and 10 we give a synthetic picture of the mean estimated values of H and δ with error bars, respectively, compared to their corresponding real values, for all IET distributions, frequency bands and percentiles. From these figures, it is easy to appreciate the better performance of H estimations with respect to the δ estimations, which display larger fluctuations and greater differences with the theoretical values. A general remark is the tendency to underestimate the real H and δ values, even if with some exceptions. This is probably related to the initial short-time transient, which usually displays a slower increase. The automatic best-fitting procedure is able to distinguish the two different regimes, but the short-time slower increase could slightly affect the fit in the long-time regime, where the real scaling exponent emerges. Interestingly, looking at Table 6 it is clear that the estimation errors (MREs) of H in the power-law cases are comparable to the corresponding reference errors. In the best cases, some MREs are surprisingly

smaller than the reference errors. Conversely, in the exponential case, the MRE is larger or much larger than the reference error.

Case	MRE H (\pm STD) Reference Errors	MRE H (\pm STD) Best Case	MRE H (\pm STD) Worst Case
Exponential	0.0052 (\pm 0.0042)	0.010 (\pm 0.010)	0.038 (\pm 0.017)
Power-Law ($\mu = 2.3$)	0.088 (\pm 0.040)	0.064 (\pm 0.040)	0.10 (\pm 0.064)
Power-Law ($\mu = 2.5$)	0.040 (\pm 0.030)	0.040 (\pm 0.020)	0.12 (\pm 0.054)
Power-Law ($\mu = 2.7$)	0.070 (\pm 0.040)	0.018 (\pm 0.013)	0.071 (\pm 0.021)

(a) H Relative Errors

Case	MRE δ (\pm STD) Reference Errors	MRE δ (\pm STD) Best Case	MRE δ (\pm STD) Worst Case
Exponential	0.024 (\pm 0.011)	0.056 (\pm 0.050)	0.12 (\pm 0.084)
Power-Law ($\mu = 2.3$)	0.040 (\pm 0.035)	0.040 (\pm 0.024)	0.17 (\pm 0.040)
Power-Law ($\mu = 2.5$)	0.062 (\pm 0.021)	0.17 (\pm 0.018)	0.28 (\pm 0.065)
Power-Law ($\mu = 2.7$)	0.15 (\pm 0.030)	0.13 (\pm 0.090)	0.25 (\pm 0.088)

(b) δ Relative Errors

Table 6: Comparison of MRE for H and δ estimated from RTEs detected with the RTEF algorithm versus corresponding reference errors, i.e., relative errors of H and δ estimated from the real RTEs. (a) Reference Errors in H versus the best and worst estimated H from detected RTEs; (b) Reference Errors in δ versus the best and worst estimated δ from detected RTEs.

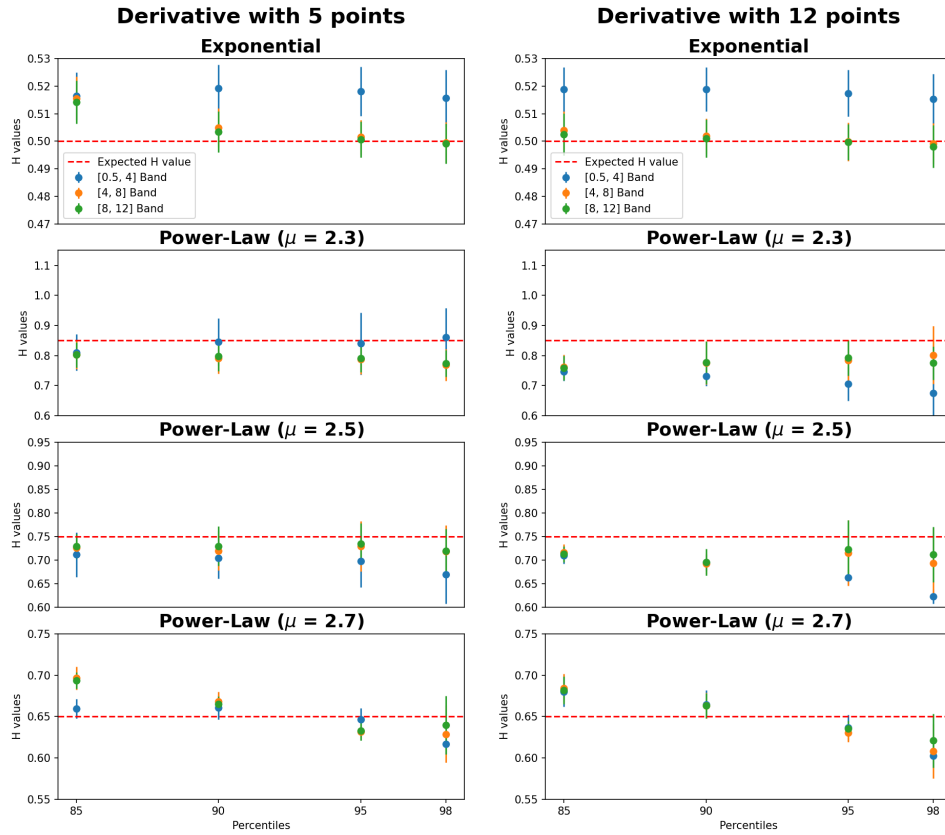


Figure 9: Mean estimated H values with error bars for each IET distribution and frequency band vs percentile values. Both $N_d = 5$ and $N_d = 12$ cases are reported. The dashed red lines represent the theoretical H values: 0.5 for the Exponential Distribution, 0.85 for Power-Law distribution with $\mu = 2.3$, 0.75 for $\mu = 2.5$, and 0.65 for $\mu = 2.7$.

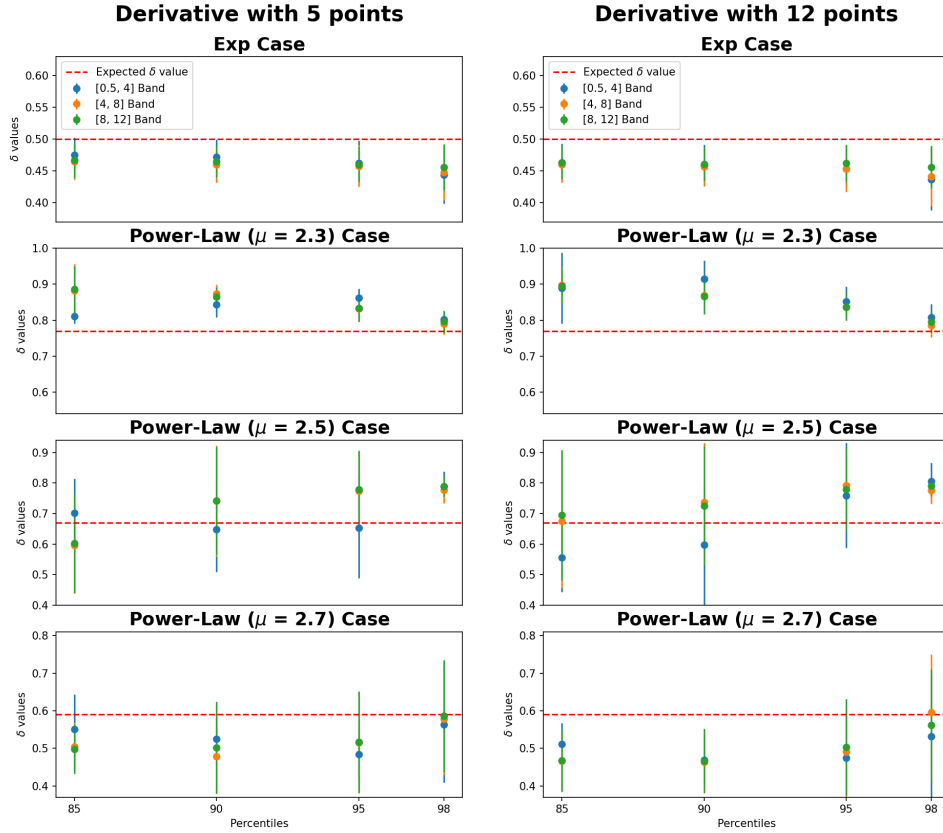


Figure 10: Mean estimated δ values with error bars for each IET distribution and frequency band vs percentile values. Both $N_d = 5$ and $N_d = 12$ cases are reported. The dashed red lines represent the theoretical δ values: 0.5 for the Exponential Distribution, ~ 0.77 for Power-Law distribution with $\mu = 2.3$, ~ 0.67 for $\mu = 2.5$, and ~ 0.59 for $\mu = 2.7$.

When looking at the RTE counting, the best accuracy in RTE detection seems to come from the higher percentiles, in particular the 98th one (see Fig. 8). Then, we would not expect to find good performances in the evaluation of complexity indices when the number of estimated RTEs is very high concerning the number of real

RTEs in the signal. Surprisingly, Tables 3, 4 and 5 show that, for power-law IET distributions, better results for the diffusion scaling exponent H are usually obtained for smaller percentiles (85, 90), even if the application of the algorithm results in a very high number of false positives. Conversely, the 98th percentile, which better approximates the RTE counts, gives the worst performances in the H evaluation⁹. Actually, power-law cases see an improvement in the estimate of H as the percentile decreases and, therefore, as the number of false positives increases (see, e.g., Tables 3, 4 and 5), while an opposite trend is seen in the exponential case (see Table 2). In the last case, the H estimation gets worse as the percentile decreases in [4, 8] and [8, 12] bands and remains about the same in the [0.5, 4] band.

Conversely, the trend in the δ evaluation is more intricate, with estimates either getting worse as the percentile decreases or remaining about the same in the power-law case. The only exception we found is given by $\mu = 2.7$, where the δ estimation improves as the percentile decreases. This last result is similar to the exponential case: δ evaluation improves as percentile decreases, that is, as the number of false positives increases. Generally speaking, the exponential case shows the best performances in the evaluation of all parameters, i.e., not only H and δ , but also the direct estimation of r_p . This is an expected result, as the exponential distribution has not a strong tail, so that the rare events have a negligible probability, being most of the IET included in 2-3 times the average IET $\langle \tau_p \rangle = 1/r_p$.

On the contrary, the opposite trends of both H and δ estimation accuracy in the exponential case with respect to the inverse power-law distributed IETs are somewhat surprising and are surely related to the very low probability of large IETs of the

⁹A slight worsening in accuracy is only seen for $\mu = 2.7$, bands [4, 8] and [8, 12], when passing from 90th to 85th percentiles.

exponential distribution. Moreover, we observe that being theoretically $H = \delta = 0.5$ in this case, the relative errors are mostly affected by limitations of the fitting procedure.

In general, it is important to underline that, in all cases, the mean relative errors in the δ estimation are much higher than in the H estimation. In fact, being based on the computation of distribution, the DE method needs a greater size of the statistical sample with respect to the DFA method, which essentially evaluates the statistical moments¹⁰. However, as proven by the authors of Ref. [64], the scaling δ is more affected by the regions around distribution maxima (the central region for single-mode distributions) and the scaling H is more affected by the distribution tails. As a consequence, δ scaling gives different information with respect to scaling H and are both needed in temporal complexity analyses, but the different level of accuracy at the same statistical sample size has to be taken into account.

In a nutshell, the main finding of the present work is that the EDDiS algorithm, which is based on the concept of event-driven diffusion scaling, is able to decrease the masking effect of false positives and, consequently, the error in the estimation of temporal complexity [17, 18]. This is in agreement with the Time Mixed Model (TMM), where a mixing of complex events and Poisson noisy events is investigated [27, 30]. However, these studies were limited to the case of a low rate of noisy events with respect to that of complex events. Here, the noisy events are given by the numerous false positives in the event-detection algorithm and, in some case, the rate of noisy events is much larger than that of the genuine complex events. This shortcoming of the event detection algorithm was here found not to compromise

¹⁰In this work the second moment, while, in the more general multifractal DFA algorithm [63], the moments of generic order q , including non-integer orders.

the possibility for the EDDiS algorithm of obtaining a good estimate of complexity, particularly of the scale of the second H moment, in the power-law case. In fact, regarding the application of DFA, the main, but counter-intuitive, result is a net improvement in the performances of complexity estimation, in the power-law case, as the number of false positives in the RTEF algorithm increases. Conversely, the trend is the opposite for the exponential case, as it would be expected for all cases.

Acknowledgements

This work was supported by the Next-Generation-EU programme under the funding schemes PNRR-PE-AI scheme (M4C2, investment 1.3, line on AI) FAIR “Future Artificial Intelligence Research”, grant id PE00000013, Spoke-8: Pervasive AI.

Authors’ contribution

Authors contributed equally to this work.

References

- [1] H. Niu, Y. Chen, B. West, Why do big data and machine learning entail the fractional dynamics ?, *Entropy* 23 (2021) 1–32. doi:10.3390/e23030297, dOI: 10.3390/e23030297.
- [2] D. C. Krakauer, Unifying complexity science and machine learning, *Front. Complex Syst.* 1 (2023) 1235202. doi:10.3389/fcpxs.2023.1235202.
- [3] P. Paradisi, G. Kaniadakis, A. M. Scarfone, The emergence of self-organization in complex systems - preface, *Chaos Soliton Fract* 81 (2015) 407–11.

- [4] S. Boccaletti, V. Latora, Y. Moreno, M. Chavez, D.-U. Hwang, Complex networks: Structure and dynamics, *Phys. Rep.* 424 (2006) 175–308. doi:10.1016/j.physrep.2005.10.009, DOI: 10.1016/j.physrep.2005.10.009.
- [5] F. Battiston, G. Cencetti, I. Iacopini, V. Latora, M. Lucas, A. Patania, J.-G. Young, G. Petri, Networks beyond pairwise interactions: Structure and dynamics, *Physics Reports* 874 (2020) 1 – 92. doi:10.1016/j.physrep.2020.05.004.
- [6] P. Ji, J. Ye, Y. Mu, W. Lin, Y. Tian, C. Hens, M. Perc, Y. Tang, J. Sun, J. Kurths, Signal propagation in complex networks, *Physics Reports* 1017 (2023) 1 – 96. doi:10.1016/j.physrep.2023.03.005.
- [7] O. Artime, M. Grassia, M. De Domenico, J. P. Gleeson, H. A. Makse, G. Mangioni, M. Perc, F. Radicchi, Robustness and resilience of complex networks, *Nature Reviews Physics* 6 (2024) 114 – 131. doi:10.1038/s42254-023-00676-y.
- [8] E. Bullmore, O. Sporns, Complex brain networks: Graph theoretical analysis of structural and functional systems, *Nature Reviews Neuroscience* 10 (2009) 186 – 198. doi:10.1038/nrn2575.
- [9] M. Rubinov, O. Sporns, Complex network measures of brain connectivity: Uses and interpretations, *NeuroImage* 52 (2010) 1059 – 1069. doi:10.1016/j.neuroimage.2009.10.003.
- [10] O. Sporns, The complex brain: connectivity, dynamics, information, *Trends in Cognitive Sciences* 26 (2022) 1066 – 1067. doi:10.1016/j.tics.2022.08.002.
- [11] M. Vaiana, S. F. Muldoon, Multilayer brain networks, *Journal of Nonlinear Science* 30 (2020) 2147 – 2169. doi:10.1007/s00332-017-9436-8.

- [12] C.-H. Yeh, D. K. Jones, X. Liang, M. Descoteaux, A. Connelly, Mapping structural connectivity using diffusion mri: Challenges and opportunities, *Journal of Magnetic Resonance Imaging* 53 (2021) 1666 – 1682. doi:10.1002/jmri.27188.
- [13] G. Chiarion, L. Sparacino, Y. Antonacci, L. Faes, L. Mesin, Connectivity analysis in eeg data: A tutorial review of the state of the art and emerging trends, *Bioengineering* 10 (2023). doi:10.3390/bioengineering10030372.
- [14] E. Borra, D. K. Jones, M. Parent, L. Petit, K. S. Rockland, R. J. Rushmore, D. Szczupak, Brain connectivity: complex, not chaotic, *Brain Structure and Function* 230 (2025). doi:10.1007/s00429-025-02943-3.
- [15] N. Laasch, W. Braun, L. Knoff, J. Bielecki, C. C. Hilgetag, Comparison of derivative-based and correlation-based methods to estimate effective connectivity in neural networks, *Scientific Reports* 15 (2025). doi:10.1038/s41598-025-88596-y.
- [16] J. Gund, Y. Mishra, B. Mallick, R. K. B. Singh, Functional switching among dynamic neuronal hub-nodes in the brain induces maintenance/transition of cognitive states, *Applied Network Science* 10 (2025). doi:10.1007/s41109-024-00688-2.
- [17] P. Grigolini, Emergence of biological complexity: Criticality, renewal and memory, *Chaos Solit. Fractals* 81 (2015) 575–88.
- [18] P. Paradisi, P. Allegrini, Intermittency-driven complexity in signal processing, in: R. Barbieri, E. P. Scilingo, G. Valenza (Eds.), *Complexity and Nonlinearity in Cardiovascular Signals*, Springer, Cham, 2017, pp. 161–195. doi:10.1007/978-3-319-58709-7-6.

- [19] A. Fingelkurts, A. Fingelkurts, C. Krause, A. Kaplan, S. Borisov, M. Sams, Structural (operational) synchrony of eeg alpha activity during an auditory memory task, *NeuroImage* 20 (2003) 529 – 542. doi:10.1016/S1053-8119(03)00305-7.
- [20] A. Y. Kaplan, A. A. Fingelkurts, A. A. Fingelkurts, S. V. Borisov, B. S. Darkhovsky, Nonstationary nature of the brain activity as revealed by eeg/meg: Methodological, practical and conceptual challenges, *Signal Processing* 85 (2005) 2190 – 2212. doi:10.1016/j.sigpro.2005.07.010.
- [21] M. I. Rabinovich, R. Huerta, P. Varona, V. S. Afraimovich, Transient cognitive dynamics, metastability, and decision making, *PLOS Computational Biology* 4 (2008) 1–9. doi:10.1371/journal.pcbi.1000072.
- [22] M. I. Rabinovich, V. S. Afraimovich, C. Bick, P. Varona, Information flow dynamics in the brain, *Physics of Life Reviews* 9 (2012) 51–73. doi:10.1016/j.plrev.2011.11.002.
- [23] A. A. Fingelkurts, A. A. Fingelkurts, C. F. Neves, Consciousness as a phenomenon in the operational architectonics of brain organization: Criticality and self-organization considerations, *Chaos, Solitons and Fractals* 55 (2013) 13–31. doi:10.1016/j.chaos.2013.02.007, emergent Critical Brain Dynamics.
- [24] M. Turalska, B. J. West, P. Grigolini, Temporal complexity of the order parameter at the phase transition, *Physical Review E* 83 (2011) 061142.
- [25] M. T. Beig, A. Svenkeson, M. Bologna, B. J. West, P. Grigolini, Critical slowing down in networks generating temporal complexity, *Physical Review E* 91 (2015) 012907.

- [26] K. Mahmoodi, S. E. Kerick, P. J. Franaszczuk, T. D. Parsons, P. Grigolini, B. J. West, Complexity synchronization in emergent intelligence, *Scientific Reports* 14 (2024). doi:10.1038/s41598-024-57384-5.
- [27] P. Paradisi, P. Allegrini, Scaling law of diffusivity generated by a noisy telegraph signal with fractal intermittency, *Chaos, Solitons and Fractals* 81 (2015) 451–462. doi:10.1016/j.chaos.2015.07.003.
- [28] D. Cox, V. Isham, *Point Processes*, Chapman and Hall, London, 1980. First CRC press reprint: 2000.
- [29] P. Allegrini, D. Menicucci, R. Bedini, L. Fronzoni, A. Gemignani, P. Grigolini, B. West, P. Paradisi, Spontaneous brain activity as a source of ideal $1/f$ noise, *Phys. Rev. E* 80 (2009). doi:10.1103/PhysRevE.80.061914, dOI: 10.1103/PhysRevE.80.061914.
- [30] P. Allegrini, D. Menicucci, R. Bedini, A. Gemignani, P. Paradisi, Complex intermittency blurred by noise: theory and application to neural dynamics, *Phys. Rev. E* 82 (2010) 015103.
- [31] E. Tagliazucchi, P. Balenzuela, D. Fraiman, D. R. Chialvo, Criticality in large-scale brain fmri dynamics unveiled by a novel point process analysis, *Frontiers in Physiology* 3 (2012) 15. doi:10.3389/fphys.2012.00015.
- [32] E. Tagliazucchi, M. Siniatchkin, H. Laufs, D. R. Chialvo, The voxel-wise functional connectome can be efficiently derived from co-activations in a sparse spatio-temporal point-process, *Frontiers in Neuroscience* 10 (2016) 381. doi:10.3389/fnins.2016.00381.

- [33] D. Cox, *Renewal Processes*, Methuen & Co., London, 1970. ISBN: 0-412-20570-X; first edition 1962.
- [34] P. Manneville, Intermittency, self-similarity and $1/f$ spectrum in dissipative dynamical systems, *J. Phys. (Paris)* 41 (1980) 1235–1243. doi:10.1051/jphys:0198000410110123500, dOI: 10.1051/jphys:0198000410110123500.
- [35] Y. Pomeau, P. Manneville, Intermittent transition to turbulence in dissipative dynamical systems, *Commun. Math. Phys.* 74 (1980) 189–197. doi:10.1007/BF01197757, dOI: 10.1007/BF01197757.
- [36] P. Allegrini, G. Aquino, P. Grigolini, L. Palatella, A. Rosa, Generalized master equation via aging continuous-time random walks, *Phys. Rev. E* 68 (2003) 561231–5612311. doi:10.1103/physreve.68.056123, dOI: 10.1103/physreve.68.056123.
- [37] M. I. Rabinovich, R. Huerta, V. Afraimovich, Dynamics of sequential decision making, *Phys. Rev. Lett.* 97 (2006) 188103. doi:10.1103/PhysRevLett.97.188103.
- [38] M. Zare, P. Grigolini, Criticality and avalanches in neural networks, *Chaos, Solitons and Fractals* 55 (2013) 80 – 94. doi:10.1016/j.chaos.2013.05.009.
- [39] M. Cafiso, P. Paradisi, Temporal complexity of a hopfield-type neural model in random and scale-free graphs, in: *Proceedings of the 16th International Joint Conference on Computational Intelligence - Volume 1:NCTA2024*, INSTICC, SciTePress, 2024, pp. 438–448. doi:10.5220/0013007600003837.
- [40] P. Paradisi, R. Cesari, A. Donateo, D. Contini, P. Allegrini, Scaling laws of diffusion and time intermittency generated by coherent structures in atmospheric

- turbulence, *Nonlinear Proc. Geoph.* 19 (2012) 113–126. P. Paradisi et al., Corrigendum, *Nonlin. Processes Geophys.* **19**, 685 (2012).
- [41] P. Grigolini, L. Palatella, G. Raffaelli, Asymmetric anomalous diffusion: an efficient way to detect memory in time series, *Fractals* 9 (2001) 439–449.
- [42] J. Klafter, A. Blumen, M. Shlesinger, Stochastic pathway to anomalous diffusion, *Phys. Rev. A* 35 (1987) 3081–3085. doi:10.1103/PhysRevA.35.3081, dOI: 10.1103/PhysRevA.35.3081.
- [43] E. Montroll, Random walks on lattices, *Proc. Symp. Appl. Math.* 16 (1964) 193–220.
- [44] E. W. Montroll, G. H. Weiss, Random walks on lattices. II, *J Math Phys* 6 (1965) 167–181.
- [45] E. Montroll, Random walks on lattices. iii. calculation of first-passage times with application to exciton trapping on photosynthetic units, *J. Math. Phys.* 10 (1969) 753–765. doi:10.1063/1.1664902, dOI: 10.1063/1.1664902.
- [46] E. Montroll, H. Scher, Random walks on lattices. iv. continuous-time walks and influence of absorbing boundaries, *J. Stat. Phys.* 9 (1973) 101–135. doi:10.1007/BF01016843, dOI: 10.1007/BF01016843.
- [47] N. Scafetta, P. Grigolini, Scaling detection in time series: diffusion entropy analysis, *Phys. Rev. E* 66 (2002). doi:10.1103/PhysRevE.66.036130, dOI: 10.1103/PhysRevE.66.036130.
- [48] M. Shlesinger, Asymptotic solutions of continuous-time random walks, *J. Stat. Phys.* 10 (1974) 421–434. doi:10.1007/BF01008803, dOI: 10.1007/BF01008803.

- [49] J. Tunaley, Asymptotic solutions of the continuous-time random walk model of diffusion, *J. Stat. Phys.* 11 (1974) 397–408. doi:10.1007/BF01026731, dOI: 10.1007/BF01026731.
- [50] J. Tunaley, Some properties of the asymptotic solutions of the montroll-weiss equation, *J. Stat. Phys.* 12 (1975) 1–10. doi:10.1007/BF01024180, dOI: 10.1007/BF01024180.
- [51] J. Tunaley, Moments of the montroll-weiss continuous-time random walk for arbitrary starting time, *J. Stat. Phys.* 14 (1976) 461–463. doi:10.1007/BF01040704, dOI: 10.1007/BF01040704.
- [52] R. Metzler, J. Klafter, The random walk’s guide to anomalous diffusion: A fractional dynamics approach, *Physics Report* 339 (2000) 1 – 77. doi:10.1016/S0370-1573(00)00070-3.
- [53] O. Akin, P. Paradisi, P. Grigolini, Periodic trend and fluctuations: The case of strong correlation, *Phys. A* 371 (2006) 157–170.
- [54] O. Akin, P. Paradisi, P. Grigolini, Perturbation-induced emergence of poisson-like behavior in non-poisson systems, *J. Stat. Mech.: Theory Exp.* (2009) P01013. doi:10.1088/1742-5468/2009/01/P01013.
- [55] G. H. Weiss, R. J. Rubin, Random walks: theory and selected applications, *Advances in Chemical Physics* 52 (1983) 363–505.
- [56] M. Shlesinger, B. West, J. Klafter, Lévy dynamics of enhanced diffusion: Application to turbulence, *Phys. Rev. Lett.* 58 (1987) 1100–1103. doi:10.1103/PhysRevLett.58.1100, dOI: 10.1103/PhysRevLett.58.1100.

- [57] V. Zaburdaev, S. Denisov, J. Klafter, Lévy walks, *Rev. Mod. Phys.* 87 (2015) 483–530. doi:10.1103/RevModPhys.87.483, dOI: 10.1103/RevModPhys.87.483.
- [58] P. Allegrini, P. Paradisi, D. Menicucci, M. Laurino, A. Piarulli, A. Gemignani, Self-organized dynamical complexity in human wakefulness and sleep: Different critical brain-activity feedback for conscious and unconscious states, *Phys. Rev. E Stat. Nonlin. Soft Matter Phys* 92 (2015). doi:10.1103/PhysRevE.92.032808.
- [59] C.-K. Peng, S. V. Buldyrev, S. Havlin, M. Simons, H. E. Stanley, A. L. Goldberger, Mosaic organization of dna nucleotides, *Phys. Rev. E* 49 (1994) 1685–1689. doi:10.1103/PhysRevE.49.1685.
- [60] H. Hurst, Long-term storage capacity of reservoirs, *Trans. Am. Soc. Civil Eng.* 116 (1951) 770–799. doi:10.1061/TACEAT.0006518.
- [61] V. Guardabasso, G. De Nicolao, M. Rocchetti, D. Rodbard, Evaluation of pulse-detection algorithms by computer simulation of hormone secretion, *American Journal of Physiology - Endocrinology and Metabolism* 255 (1988) 18/6.
- [62] P. Allegrini, G. Aquino, P. Grigolini, L. Palatella, A. Rosa, Generalized master equation via aging continuous-time random walks, *Phys. Rev. E* 68 (2003) 056123. URL: <https://link.aps.org/doi/10.1103/PhysRevE.68.056123>. doi:10.1103/PhysRevE.68.056123.
- [63] J. W. Kantelhardt, S. A. Zschiegner, E. Koscielny-Bunde, S. Havlin, A. Bunde, H. E. Stanley, Multifractal detrended fluctuation analysis of nonstationary time series, *Physica A* 316 (2002) 87 – 114. doi:10.1016/S0378-4371(02)01383-3.
- [64] P. Allegrini, J. Bellazzini, G. Bramanti, M. Ignaccolo, P. Grigolini, J. Yang,

Scaling breakdown:a signature of aging, Physical Review E 66 (2002). doi:10.1103/PhysRevE.66.015101.